Experimental investigation of cavitation in elastomeric seismic isolation bearings

Manish Kumar* †, Andrew S. Whittaker and Michael C. Constantinou

Department of Civil, Structural and Environmental Engineering, 212 Ketter Hall, University at Buffalo, State University of New York, Buffalo, NY 14260, U.S.A.

ABSTRACT

Design standards for seismic isolation of nuclear power plants in USA will consider the effects of beyond design basis loadings, including extreme earthquakes. Seismic isolation is being considered for new build nuclear power plant construction and design of isolation systems will have to consider these extreme loadings, which includes the possibility of net tensile force in bearings under beyond design basis shaking.

A series of experiments were conducted at University at Buffalo to characterize the behavior of elastomeric bearings in tension. Sixteen low damping rubber bearings from two manufacturers, with similar geometric properties but different shear moduli, were tested under various loading conditions to determine factors that affect cavitation in an elastomeric bearing. The effect of cavitation on the shear and axial properties of elastomeric bearings was investigated by performing post-cavitation tests. The test data were used to validate a phenomenological model of an elastomeric bearing in tension, which is implemented in OpenSees, ABAQUS and LS-DYNA.

KEY WORDS: cavitation, seismic isolation, elastomeric bearings, tension, nuclear power plant

1. Introduction

There are two types of elastomeric seismic isolation bearings being implemented in the United States at this time, namely, low damping rubber (LDR) and lead rubber (LR) bearings. The LDR and LR bearings utilize low damping natural rubber as the base compound. The LR bearing is a LDR with a central lead core, which provides energy dissipation. The response of these types of elastomeric bearings in tension is assumed to be identical because the lead core does not contribute to tensile strength and stiffness.

Tensile deformation in elastomeric bearings has traditionally been considered undesirable. Design codes and standards that explicitly acknowledge response in axial tension either do not allow tensile loading or limit the value of allowable tensile stress in elastomeric bearings under design-basis loading. The Japanese specifications for design of highway bridges [1] limit the tensile stress in G8 and G10 rubber (rubber classes with shear modulus of 0.8 and 1 MPa, respectively) to 2 MPa. Eurocode 8 restricts the use of elastomeric bearings if axial tensile force is expected during seismic loadings [2]. The Chinese seismic design code limits the tensile stress to 1 MPa [3].

Experiments have shown that elastomeric bearings may sustain large tensile strains up to 100%, following cavitation, without rupture [4]. The design codes and guidelines for seismic isolation

* Correspondence to: Department of Civil, Structural and Environmental Engineering, 212 Ketter Hall, University at Buffalo, State University of New York, Buffalo, NY 14260, U.S.A.
† E-mail: mkumar2@buffalo.edu

of nuclear power plants in USA [5; 6] consider the effects of beyond design basis earthquake loadings, which may produce net tensile force in one or more bearings. Similarly, the use of isolation for tall buildings may result in tensile loading for design basis and beyond design basis shaking. The tensile properties of elastomeric bearings need to be investigated to consider tensile loading in seismic isolator design, which would enable development of robust mathematical models to capture the load-deformation behavior in tension.

The response of an elastomeric bearing under tensile loading is characterized by the formation of cavities in the volume of the rubber. Gent and Lindley [7] explained that fracture inside a rubber layer occurs at a critical hydrostatic stress value, which is related to a critical value of applied tensile stress. This critical stress, known as the cavitation stress, depends mainly on the rubber compound.

Much of the initial work on cavitation of elastomers was done by Gent and Lindley [7]. They used bonded rubber cylinders in their experiments to investigate behavior under tensile loading. The tensile behavior of bonded rubber is highly dependent on thickness, or more appropriately the shape factor, S , which is defined as the bonded rubber area divided by the perimeter area free to bulge. Shape factors in the range from 10 to 30 are practical for seismic isolation of buildings, bridges and infrastructure. Unfortunately, there is little experimental data on the behavior of elastomeric bearings in tension with shape factors in this range. A summary of the relevant experimental work is presented in Table 1. Only work on seismic isolation bearings is identified in the table and studies on bonded rubber cylinders (e.g., [8], [9]) are not described.

Table 1: Experimental work on the tensile properties of elastomeric bearings

Reference	Bearing properties	Focus
Clark [10]	HDR, diameter 176 mm, shape factor~ 20	Monotonic tensile failure
Iwabe *et al.* [4]	LDR, LR, HDR bearings, diameter 500 mm and 1000 mm, shape factor ~30	Tension, shear-tension, post-cavitation mechanical properties
Kato *et al.* [11]	LDR, diameter 500 mm and 1000 mm, varying bearing plate thickness, shape factor~33	Tension, scale effect, bearing plate thickness
Shoji *et al.* [12]	LR, 240×240 mm, shape factor~8	Cyclic deterioration under tension
Feng *et al.* [13]	LR, diameter 100 mm, shape factor~15	Tension, mechanical properties, three-dimensional dynamic loading
Warn [14]	LDR, LR, outer diameter 152 mm, inner diameter 30 mm, shape factor~12	Tension, coupling of horizontal and vertical motion
Constantinou *et al.* [15]	LDR, diameter 250 mm, shape factor~9	Single cycle tensile loading

Figure 1 and Figure 2 present the behavior of LDR bearings in pure tension and in tension with co-existing shear, respectively.

Some of the important conclusions of these experimental studies were:

1. A substantial reduction of tensile stiffness occurs at a critical tensile stress (cavitation stress), which depends on the shear modulus and shape factor.
2. The load-deformation behavior in tension is linear up to cavitation with the tensile stiffness approximately equal to the compressive stiffness, followed by nonlinear post-cavitation behavior.
3. Tension coupled with shear loading increases the tensile load and deformation capacity of a bearing when compared to pure tension.

4. Under cyclic loading the tensile strength decreases, and the extent of the reduction is a function of the maximum tensile strain experienced in previous cycles.
5. The state of tension during shear loading has minimal effect on shear stiffness and shear hysteresis loops.

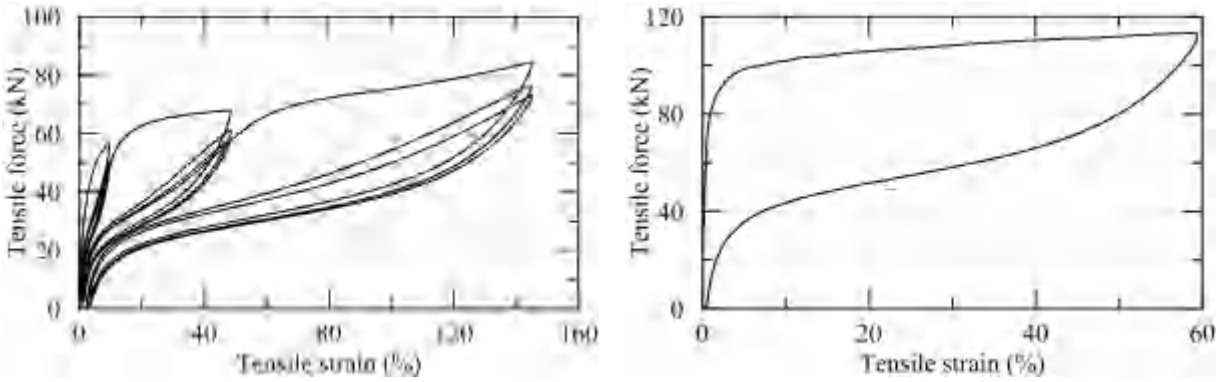

a) Warn [14] b) Constantinou *et al.* [15]

Figure 1: Load-deformation behavior of LDR bearing under cyclic tension

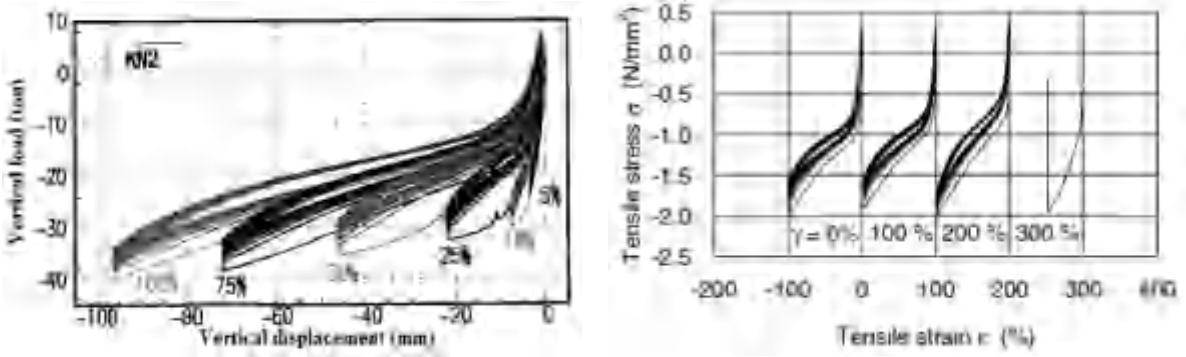

a) 200% lateral offset [4] b) Varying lateral offset [11]

Figure 2: Load-deformation behavior of LDR bearings in cyclic tension with lateral offset

The behavior of elastomeric bearings under cyclic tensile loading is described in detail in Kumar *et al.* [16] and a phenomenological model was proposed to model such behavior. The model was validated using the data described in this paper, and included in models of elastomeric bearings now available in OpenSees [17], ABAQUS [18] and LS-DYNA [19].

2. Experimental plan

2.1 Model Bearing Properties

The geometric and material properties of the model bearings were based on considerations of a) elastomers used in seismic isolation bearings, b) commercially available rubber sheet thickness, c) available molds for fabricating bearings, d) axial load capacity of the Single Bearing Testing Machine (SBTM) at the University at Buffalo, and e) bending moment capacity of the triaxial load cell in the SBTM. The physical limitations of the SBTM limited the diameter of the bearings to 300 mm and the total rubber thickness to approximately 150 mm, enabling the application of significant axial pressures and shearing strains. The target shape factors were 10 and 20.

Two manufacturers, Dynamic Isolation Systems, Inc. (DIS) and Mageba, each provided eight bearings for the experiments. The bonded diameter, shear modulus, and cover rubber thickness of the bearings differed by manufacturer; the DIS bearings had a central hole[‡]. Each set of eight bearings had the same diameter, with two shape factors per set. The rubber layer thickness was either 7 mm (A) or 4 mm (B). The bearings were identified as DA1, DB1, MA1, MB1 etc., where the first letter refers to the manufacturer (D for DIS and M for Mageba), the second letter identifies the rubber layer thickness (or shape factor), and the number identifies the specific bearing. For example, bearing DA1 was manufactured by DIS with a rubber layer thickness 7 mm.

The effective shear modulus, G, of a bearing was determined experimentally at 100% shear strain, and was used to calculate the mechanical properties of a bearing. The shape factor, S, of the bearings with (DA and DB) and without (MA and MB) a central hole is calculated using:

$$S = \frac{D_o - D_i}{4t_r} : \text{with central hole} \qquad S = \frac{D_o}{4t_r} : \text{without a central hole} \tag{1}$$

where D_o is the outer diameter excluding the cover thickness; D_i is the internal diameter; and t_r is the thickness of single rubber layer. The moment of inertia, I, and the compression modulus, E_c, is calculated as:

$$I = \frac{\pi}{64}\left[\left(D_o + t_c\right)^4 - D_i^4\right] \qquad E_c = \left(\frac{1}{6GS^2F} + \frac{4}{3K}\right)^{-1} \tag{2}$$

where t_c is added to the outer diameter to include a contribution from half of the cover rubber thickness to the moment of inertia (this is a common assumption made for small size bearings to approximate the effect of the cover rubber); F is a factor to account for the central hole in a circular bearing [15]; and K is the bulk modulus of rubber, which is assumed to be 2000 MPa: the default value in seismic isolation specifications (e.g., [21], [22])[§].

The vertical stiffness in compression and in tension prior to cavitation, K_{v0}, and the horizontal stiffness, K_{H0}, are given by:

$$K_{v0} = \frac{AE_c}{T_r} \qquad K_{H0} = \frac{GA}{T_r} \tag{3}$$

where A is the bonded rubber area of a bearing; and T_r is the total thickness of rubber layers in a bearing. The critical buckling load, P_{cr}, and the critical displacement, u_{cr}, in compression are:

[‡] Results of tensile tests on elastomeric bearings with a central hole are likely better correlated to the behavior of LR bearing in tension than tests on bearings without a hole [20].

[§] Reported values of bulk modulus vary from 1000 MPa to 3500 MPa (e.g., [23], [24], [25], [26]). The wide range is due to the different methods used to estimate the modulus and the errors in those experiments. The recent study of Kelly and Lai [22], which back-calculated the modulus from bearing tests, estimated K = 2300 MPa, which supported the use of 2000 MPa here.

$$P_{cr} = \sqrt{P_E GA_S} = \frac{\pi\sqrt{E_r GIA}}{T_r} \qquad u_{cr} = \frac{P_{cr}}{K_{v0}} \tag{4}$$

where A_S is the shear area and E_r is the rotational modulus of a bearing. The cavitation force, F_c, and cavitation displacement, u_c, in tension are:

$$F_c = 3GA \qquad u_c = \frac{F_c}{K_{v0}} \tag{5}$$

The geometric and material properties of the four types of rubber bearings and their estimated mechanical properties are summarized in Table 2.

Table 2: Geometrical and mechanical properties of elastomeric bearings

Property	Notations (units)	DA	DB	MA	MB
Single rubber layer thickness	t_r (mm)	7	4	7	4
Number of rubber layers	n	20	20	20	20
Total rubber layer thickness	T_r (mm)	140	80	140	80
Steel shim thickness	t_s (mm)	3	3	3	3
Outer diameter	D_o (mm)	297	297	299	299
Inner diameter	D_i (mm)	19	19	0	0
Cover thickness	t_c (mm)	4	4	5	5
Bonded area (including cover)	A (mm^2)	70778	70778	72583	72583
Shear modulus[1]	G (MPa)	0.41	0.45	0.79	0.77
Shape factor (without cover)	S	9.9	17.4	10.7	18.7
Vertical stiffness	K_{v0} (kN/m)	80161	377341	205999	705255
Horizontal stiffness	K_{H0} (kN/m)	207	398	410	699
Critical buckling load	P_{cr} (kN)	557	1675	1266	3060
Critical buckling displacement	u_{cr} (mm)	6.9	4.4	6.1	4.3
Cavitation force	F_c (kN)	87	96	172	168
Cavitation displacement	u_c (mm)	1.1	0.3	0.8	0.2

1. Determined from experiments at 100% shear strain

2.2 Test Program

The six objectives of the test program were to understand and characterize:

1. Cavitation and post-cavitation behavior of elastomeric bearings under tensile loading
2. Effect of loading history on tensile properties
3. Change in shear and compression properties following tensile loading
4. Influence of shear displacement on tensile force-displacement response
5. Effect of cavitation on buckling load capacity

These objectives were accomplished through a series of tests on low damping rubber (LDR) bearings in the axial and shear directions. Five types of test were conducted:

1. *Characterization tests*: Mechanical properties of the bearings were determined from benchmark tests in shear and compression. The shear characterization tests were conducted at 100% shear strain under a nominal axial pressure of 1 MPa. This value of axial load allowed the bearings to undergo shear strains greater than 100% without exceeding the moment capacity of the triaxial load cell. It would be established later from experiments that mechanical properties (e.g., shear modulus and axial stiffness) does not significantly change with axial loads. Force-controlled compression characterization tests were conducted at amplitude of 300 kN (4.3 MPa).
2. *Effect of lateral offset on behavior in tension*: Tests were conducted to understand the effects of lateral offset on the pre-cavitation and post-cavitation behavior of elastomeric bearings. Force-controlled tests were conducted at an amplitude equal to the half of the estimated cavitation strength to obtain the variation of tensile stiffness with lateral offset. Tests involving cavitation were also conducted at different lateral offsets under displacement control to investigate the effect of lateral offset on cavitation properties, namely, cavitation strength, post-cavitation stiffness, and strength degradation.
3. *Effect of shear loading history on cavitation*: Loading history in the shear direction might affect the cavitation behavior of an elastomeric bearing. Two model bearings were subjected to shear displacement histories of a varying number of cycles and amplitudes followed by cyclic tensile loading.
4. *Effect of tensile loading history on cavitation*: The effect of tensile loading history on cavitation was investigated using two triangular excitation signals: 1) increasing displacement amplitude after every three cycles (IT), and 2) decreasing amplitude after every three cycles (DT).
5. *Effect of cavitation on critical buckling load capacity*: Bearings were subjected to linearly increasing compressive loads up to failure to assess the effect of cavitation on the subsequent critical buckling load at zero lateral displacement.

The summary of the testing program is presented in Table 3. A summary of the sequence of loading is summarized in Figure 3. The detailed sequence is presented in Kumar [20].

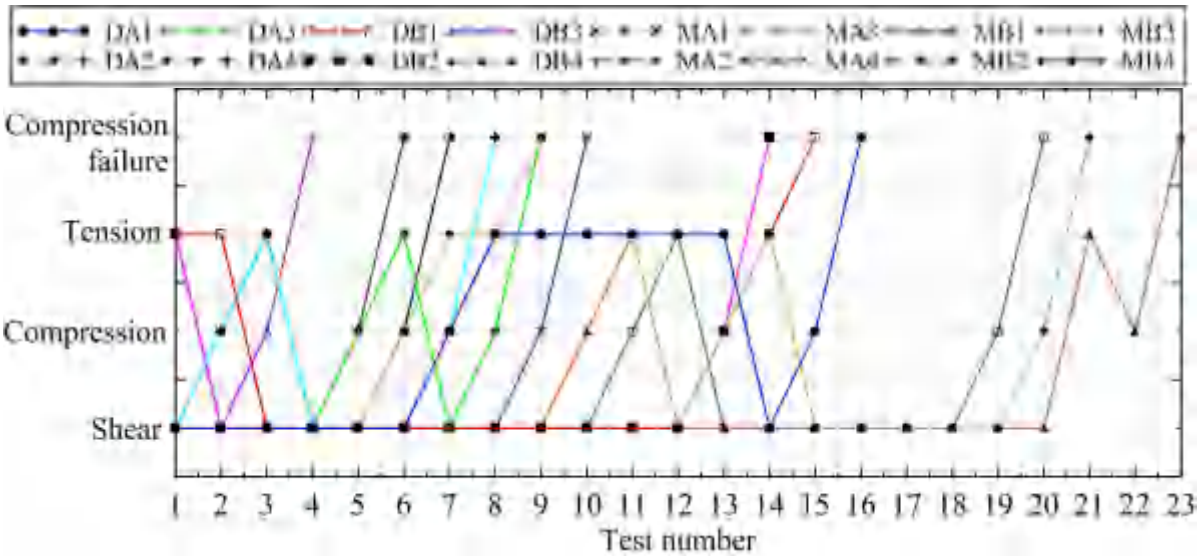

Figure 3: Loading sequence of elastomeric bearings

Table 3: Summary of single bearing testing program

Test	Bearing	Type	Signal[1]	Preload P_0 (kN)	Axial load amplitude[2] (kN)	Static lateral offset Δ/R (%)	Disp. amplitude $_u$, δ(%)	Freq. f (Hz)	No. of cycles
1. Characterization tests									
1	DA1, MA1	Shear	S	70	n.a.	n.a.	±25, ±50, ±75, ±100	0.01	4
2	MB1, DB4	Shear	S	70	n.a.	n.a.	±25, ±50, ±100, ±125, ±175	0.01	4
3	DB1, MB1, DB4	Shear	S	35, 70, 105, 140, 175	n.a.	n.a.	±100	0.01	4
4	DA4	Shear	S	11, 22, 33, 44, 70, 90, 140	n.a.	n.a.	±100	0.01	4
5	DA1, MA1	Shear	S	70	n.a.	n.a.	±25, ±50, ±75	0.1	4
6	DA1, MA1	Tension	T	0	-25	n.a.	n.a.	0.01	4
7	All	Shear	S	70	n.a.	n.a.	±100	0.01	4
8	All	Compression	T	0	300	n.a.	n.a.	0.01	4
2. Effect of lateral offset on behavior in tension									
1	DA1, MA1	Tension	T	0	-50 kN	0, 50, 100, 150, 200	n.a.	0.01	4
2	DA4, MA4	Tension	T	0	-50 kN	0, 25, 50, 75, 100	n.a.	0.01	4
3	DB1, DB2	Tension	IT	0	n.a.	100	5, 10, 25, 50, 100	0.01	3
4	DB1, DB2	Shear	S	35, 70, 105, 140, 175	n.a.	n.a.	±100	0.01	4
5	DB1, DB2	Shear	S	70	n.a.	n.a.	±25, ±50, ±100, ±125, ±175	0.01	4
6	DA4,MA4	Tension	IT	0	n.a.	0	5, 10, 25, 50, 65	0.01	3
7	DA4, MA4	Shear	S	70	n.a.	n.a.	±100	0.01	4
8	DA4, MA4	Compression	T	0	300	n.a.	n.a.	0.01	4
3. Effect of shear loading history on cavitation									
1	MB1, MB2, DB4	Tension	IT	0	n.a.	0	5, 10, 25, 50, 100	0.01	3
2	MB4	Tension	DT	0	n.a.	0	100, 50, 25, 10, 5	0.01	3
3	MB1, DB4	Shear	S	35, 70, 105, 140, 175	n.a.	n.a.	±100	0.01	4
4	DB4	Shear	S	70	n.a.	n.a.	±25, ±50, ±100, ±125, ±175	0.01	4
5	MB2, MB4	Shear	S	70	n.a.	n.a.	±100	0.01	4
6	MB2, MB4	Compression	T	0	300	n.a.	n.a.	0.01	4
4. Effect of tensile loading history on cavitation									
1	DA3, MA3	Tension	DT	0	n.a.	0	50, 25, 10, 5	0.01	3
2	DA3, MA3	Shear	S	70	n.a.	n.a.	±100	0.01	4
3	DA3, MA3	Compression	T	0	300	n.a.	n.a.	0.01	4
4	DA3, MA3	Tension	IT	0	n.a.	0	5, 10, 25, 50, 65	0.01	3
5	DA3, MA3	Shear	S	70	n.a.	n.a.	±100	0.01	4
6	DA3, MA3	Compression	T	0	300	n.a.	n.a.	0.01	4
7	DA2, MA2	Tension	IT	0	n.a.	0	5, 10, 25, 50, 65	0.01	3
8	DA2, MA2	Shear	S	70	n.a.	n.a.	±100	0.01	4
9	DA2, MA2	Compression	T	0	300	n.a.	n.a.	0.01	4
10	DA2, MA2	Tension	DT	0	n.a.	0	65, 50, 25, 10, 5	0.01	3
11	DA2, MA2	Shear	S	70	n.a.	n.a.	±100	0.01	4
12	DA2, MA2	Compression	T	0	300	n.a.	n.a.	0.01	4
13	DB3, MB3	Tension	IT	0	n.a.	0	5, 10, 25, 50	0.01	3
14	DB3, MB3	Shear	S	70	n.a.	n.a.	±100	0.01	4
15	DB3, MB3	Compression	T	0	300	n.a.	n.a.	0.01	4
16	DB3, MB3	Tension	DT	0	n.a.	0	50, 25, 10, 5	0.01	3
17	DB3, MB3	Shear	S	70	n.a.	n.a.	±100	0.01	4
18	DB3, MB3	Compression	T	0	300	n.a.	n.a.	0.01	4
5. Effect of cavitation on critical buckling load capacity									
1	ALL	Compression	L	0	n.a.	0	Failure	n.a.	n.a.

1. S = Sinusoidal, T = Triangular, IT = Increasing Triangular, DT = Decreasing Triangular

2. Negative value indicates loading in tension

The amplitude and frequency of the signals varied for different tests. Tensile tests that involved cavitation were conducted under displacement control using Increasing Triangular (IT) and Decreasing Triangular (DT) signals. The displacement amplitude was increased and decreased in IT and DT, respectively, after three cycles. Shear characterization tests were conducted under displacement control using a Sinusoidal (S) signal. Compression and tensile characterization tests were conducted under force control using a Triangular (T) signal. Most of the experiments were quasi-static tests conducted at an excitation frequency of 0.01 Hz. Some characterization tests were also conducted at a frequency of 0.1 to investigate the effects of loading rate on mechanical properties. A linear (L) signal was used to conduct the compression failure tests. Illustrations of the input signals to the actuators are presented in Figure 4.

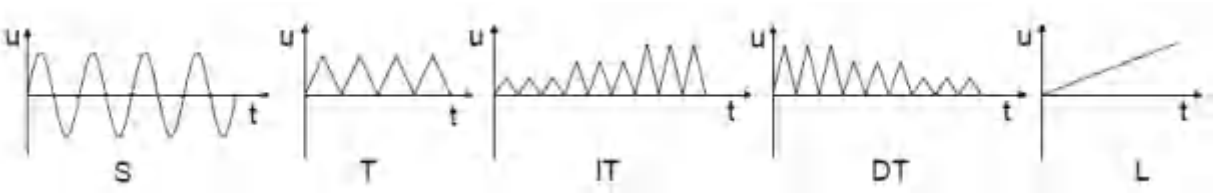

Figure 4: Signals used in the experiment

3. Experimental set up

A Single Bearing Testing Machine (SBTM) was used to perform tensile tests and shear and compression characterization tests. The compression failure tests were performed using a Concrete Strength Tester (CST).

For tests performed using the SBTM, twelve data channels were used to record the performance of the actuators and the response of the seismic isolation bearing. Nine of these data channels were stationary instruments, and one data channel recorded time. Two data channels were used to measure relative vertical displacement across the bearing. The deformations in the bearings were also measured using a Krypton camera [27] that tracked the locations of seven LEDs installed on bearings. Five video cameras were used to record the tests.

The SBTM is used to test single elastomeric bearing under unidirectional shear and axial loading. The SBTM consists of a pedestal frame, a reaction frame, a loading beam, a horizontal (dynamic) MTS™ actuator, two vertical Parker actuators and a 5-channel reaction load cell. The SBTM can impose shearing and axial loads and displacements, and combinations thereof. The actuators' capacities in terms of maximum stroke, velocity, and force are presented in Table 4. A schematic of the SBTM showing its dimensions and using standard U.S. section sizes is presented in Figure 5. Figure 6 presents its spatial orientation. Figure 7 is a photograph of the SBTM during operation.

Table 4: Single bearing testing machine actuators capabilities

Actuator[1]	Stroke (mm)	Velocity (mm/s)	Force (kN)
Horizontal (MTS)	±152	635	245
North vertical (Parker)	±50	50	317 Compression, 300 Tension
South vertical (Parker)	±50	50	317 Compression, 300 Tension

1. Actuator orientation is shown in Figure 6

Six data channels were used for the compression failure tests in the CST. Five of these channels were stationary instruments, and one data channel recorded time. The stationary instruments

included four linear potentiometers and one load cell to measure axial displacement and axial force, respectively. The stroke of each linear potentiometer was ± 25 mm. Figure 8 is photograph of the CST during operation.

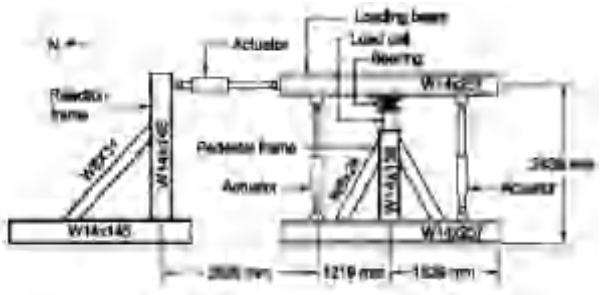

Figure 5: Schematic of Single Bearing Testing Machine [28]

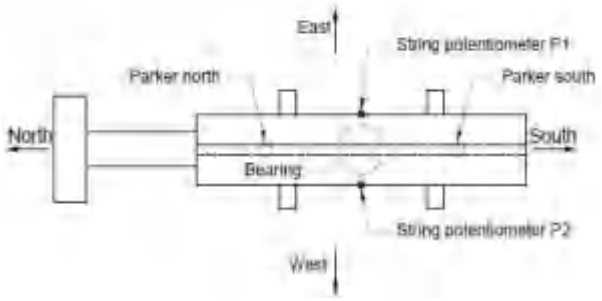

Figure 6: Layout of experimental setup (top-view)

Figure 7: Single Bearing Testing Machine

Figure 8: Concrete Strength Tester

For tests involving combined shear and axial loading, the vertical and horizontal actuators rotate in their respective planes and this was considered in the calculation of the forces on a bearing. The shear force was obtained by subtracting the horizontal component of vertical actuator force from the force measured in the horizontal actuator. The axial load of a bearing was obtained from the reaction load cell. Kumar [20] presents detailed information on the procedures used to reduce and process data from the experiments.

4. Experimental Results

4.1 Characterization Tests

4.1.1 Shear Properties

The benchmark shear tests were performed at 75% or 100% shear strain[**] at an axial load of 70 kN, which corresponded to an axial pressure of approximately 1 MPa. An idealized force-displacement curve for the behavior of elastomeric seismic isolation bearings in shear is presented in Figure 9. The effective shear stiffness is calculated as:

[**] DIS type A and B and Mageba type B bearings were tested at 100% shear strain. Mageba type A bearings were tested at 75% shear strain due to physical limitations of the SBTM. See Kumar [20] for details.

$$K_{eff} = \frac{|F_{\max}| + |F_{\min}|}{|u_{\max}| + |u_{\min}|} \tag{6}$$

where u_{max} and u_{min} are the maximum and the minimum shear displacements, and F_{max} and F_{min} are the corresponding forces, as shown in the Figure 9. The effective shear modulus is:

$$G_{eff} = \frac{K_{eff} T_r}{A} \tag{7}$$

where T_r is the total thickness of the rubber layers, and A is the bonded rubber area that includes one half of the cover rubber thickness. The characteristic strength, Q_d, is estimated as:

$$Q_d = \frac{|F^+(u=0)| + |F^-(u=0)|}{2} \tag{8}$$

where $F^+(u=0)$ and $F^-(u=0)$ are the positive and negative zero displacement force intercepts, respectively, on the shear force-displacement hysteresis curve.

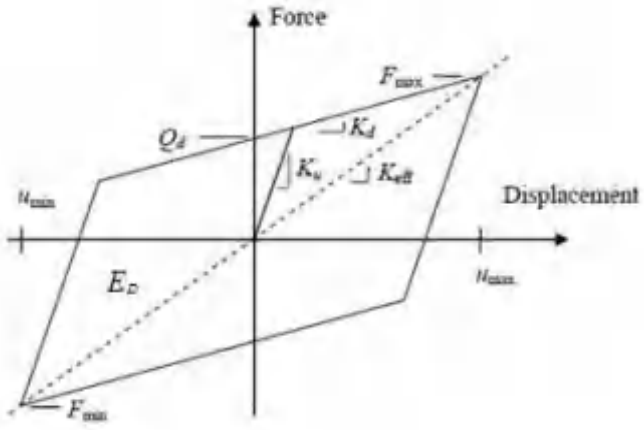

Figure 9: Idealized force-displacement behavior of an elastomeric bearing in shear [29]

The effective damping in shear is calculated as:

$$\beta_{eff} = \frac{2}{\pi}\left[\frac{E_D}{K_{eff}\left(|u_{\max}| + |u_{\min}|\right)^2}\right] \tag{9}$$

where E_D is the energy dissipated per cycle. For a LDR bearing, the characteristic shear strength is estimated as:

$$Q_d = \frac{\pi}{2}\beta_{eff} K_{eff} D \tag{10}$$

where D is the displacement at which β_{eff} and K_{eff} are calculated.

The shear properties are calculated as average of the first three cycles for each bearing, and the average shear properties of four bearings for each bearing type are summarized in Table 5. Post-cavitation values of the shear properties are not included. The differences between the experimental and theoretical value of the characteristic strength obtained using (8) and (10), respectively, are small.

Table 5: Average shear properties of bearings

Bearing type	K_{eff} (kN/mm)	G_{eff} (MPa)	β_{eff} (%)	Q_d (kN)		
				Experimental	Theoretical	Difference (%)
DA	0.205	0.41	4.2	2.0	1.9	5
DB	0.398	0.45	3.1	1.6	1.6	0
MA	0.408	0.79	3.5	3.2	3.1	3
MB	0.700	0.77	3.8	3.2	3.4	6

The effect of the forcing frequency on shear modulus was investigated by performing shear characterization tests on bearing MA1 at 0.01 Hz and 0.1 Hz. No change in shear modulus was observed with frequency.

Shear characterization tests, in addition to benchmark shear tests, were conducted. The variations of shear modulus with shear strain and axial pressure are presented in Figure 10 and Figure 11, respectively. The suffixes in the legend entries refer to pre- and post-cavitation values. Pre- and post-cavitation tests were not performed on all bearings, because the experimental program had multiple objectives, each requiring a different protocol.

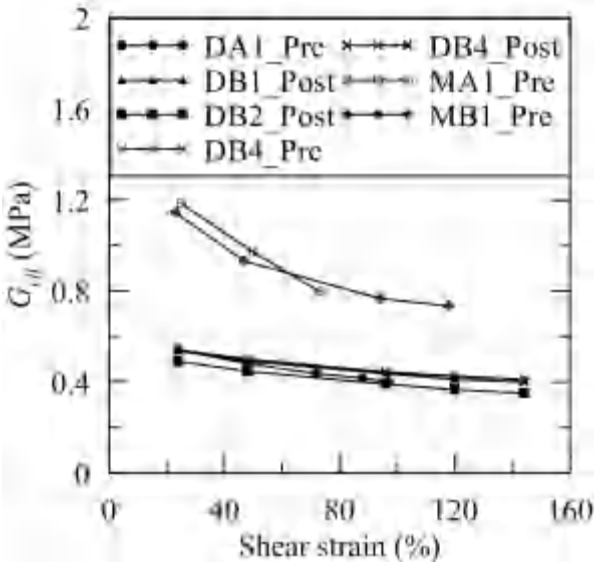

Figure 10: Variation of effective shear modulus with shear strain

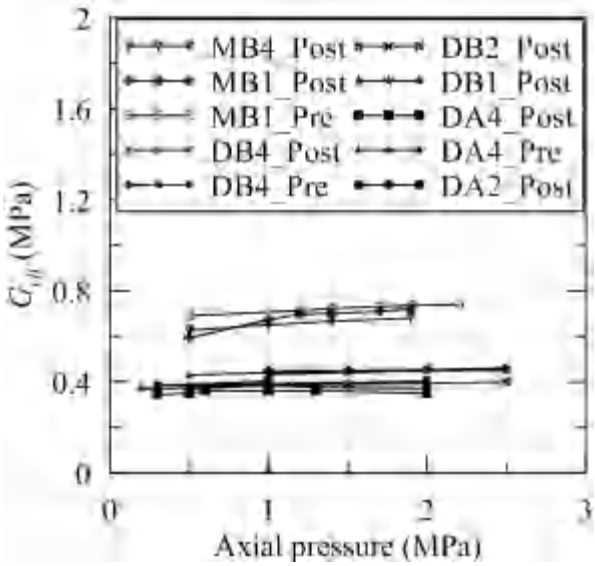

Figure 11: Variation of effective shear modulus with axial pressure

Shear modulus decreases with increasing shear strain, which is consistent with observations from past experiments. It has been observed that the shear modulus of the rubber in elastomeric bearings decreases up to a moderate shear strain, remains constant, and then increases at high values of shear strain (e.g, [10], [15], [30], [16]). The variation of shear modulus with shear strain could only be obtained up to a shear strain of 150%, limited by the moment capacity of the

five-channel load cell. No change in shear modulus is observed with axial pressure.

4.1.2 Compression Properties

The compressive stiffness of all bearings is determined using benchmark compression tests in which bearings were subjected to force-controlled triangular cyclic loading of amplitude 300 kN corresponding to an axial pressure of 4.3 MPa. The vertical stiffness, K_{v0}, is calculated as [28]:

$$K_{v0} = \frac{P^{+} - P^{-}}{\delta^{+} - \delta^{-}} \tag{11}$$

where P^{+} is an axial compressive load corresponding to a target pressure (p) plus an offset Δp, and P^{-} is an axial compressive load corresponding to $p - \Delta p$, and δ^{+} and δ^{-} are the vertical deformations corresponding to P^{+} and P^{-}, respectively, on the ascending branch of the hysteresis loop. The values of p and Δp are chosen as 2 MPa and 1.5 MPa, respectively.

The effective damping in the vertical direction, β_v, is estimated using [28]:

$$\beta_v = \frac{E_D}{2\pi(|P_{\max} - P_{\min}|)(|\delta_{\max} - \delta_{\min}|)} \tag{12}$$

where $\delta_{\max}$ and $\delta_{\min}$ are the maximum and minimum vertical deformations, and $P_{\max}$ and $P_{\min}$ are the corresponding axial loads, respectively; E_D, is the energy dissipated per cycle.

The compression properties are calculated as average of the first three cycles for each bearing, and the average compression properties of four bearings for each bearing type are summarized in in Table 6. The averaged properties do not include post-cavitation values of the compression properties. The theoretical values of compression stiffness are calculated using (3) for each bearing type and are compared with experimental values in Table 6. The average shear moduli from Table 5 are used for calculations of compression stiffness. The theoretical predictions are similar to the experimental results with differences less than 10% except for type MA.

Table 6: Average compression properties of bearings

Bearing	K_{v0} (kN/mm)			β_v (%)
	Experimental	Theoretical	Difference (%)	
DA	75	80	7	1.1
DB	355	377	6	1.0
MA	235	206	12	1.4
MB	727	705	3	2.0

4.1.3 Tensile Properties

The benchmark tensile characterization tests were performed on two bearings. Bearings were subjected to a force-controlled triangular loading of amplitude 25 kN. The amplitude was chosen as approximately a quarter of the estimated cavitation strength to ensure that no cavitation occurs during these tests. The tensile properties of the remaining bearings were obtained from other tensile tests. Behavior in tension is affected only by past damage induced by tensile loading. If there is no prior damage, behavior in tension does not depend on loading protocol.

The tensile properties of the bearings obtained using the load-deformation cycles of Figure 12 are summarized in Table 7. The mechanical properties associated with the first tensile load-deformation cycle are presented. All the bearings in Figure 12 are subjected to the increasing triangular signal under displacement control, except for DA1 and MA3, which are subjected to a triangular signal under force control and a decreasing triangular signal under displacement control. The cavitation strength is defined as the force at the intersection of the lines of pre- and post-cavitation stiffness. The tensile stiffness and damping ratio were obtained using (11) and (12). The values of p and Δp were 0.3 MPa and 0.25 MPa, respectively.

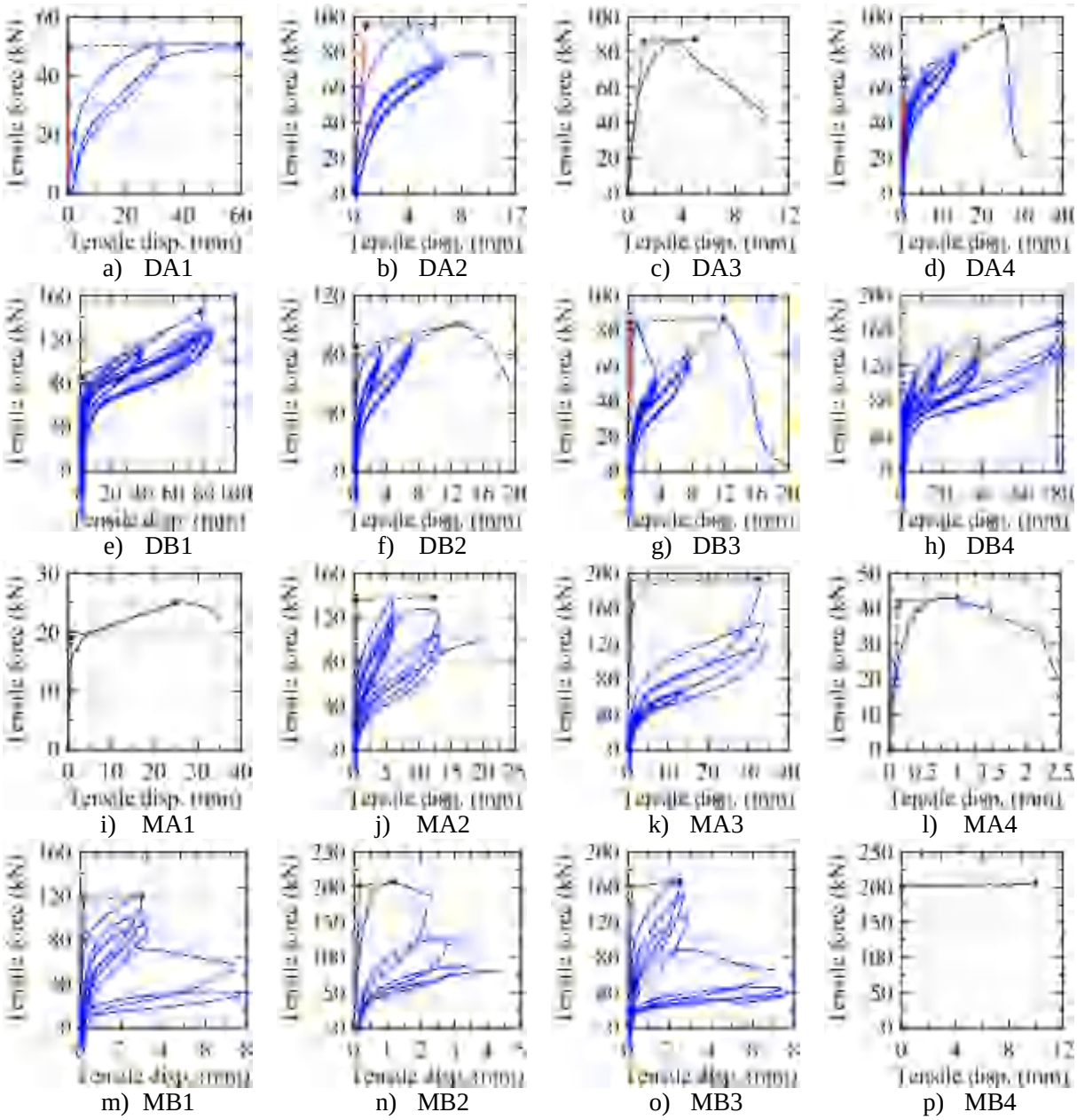

a) DA1 b) DA2 c) DA3 d) DA4

e) DB1 f) DB2 g) DB3 h) DB4

i) MA1 j) MA2 k) MA3 l) MA4

m) MB1 n) MB2 o) MB3 p) MB4

Figure 12: Calculation of the tensile properties of bearings

Table 7: Tensile properties of the elastomeric bearings

Bearing	Test	Δ / R	K_{v0} (kN/mm)	F_c (kN) Experimental	F_c (kN) Theoretical			$\frac{F_c \text{ (experimental)}}{F_c \text{ (theorerical)}}$
					G_{eff} (MPa)	A (mm^2)	$3GA$	
DA1[1]	13	2.0	111	50	0.40	70778	85	0.59
DA2	3a	0	103	95	0.42	70778	90	1.06
DA3	3	0	76	86	0.42	70778	88	0.97
DA4[1]	14	0	65	65	0.38	70778	81	0.80
DB1[2]	14	0	138	85	0.44	70778	93	0.91
DB2[1]	1	1.0	217	85	0.39	70778	83	1.03
DB3	1a	0	239	85	0.41	70778	87	0.98
DB4	11a	0	274	110	0.45	70778	96	1.15
MA1	8	0	25	19	0.80	72583	173	0.11
MA2	3	0	296	136	0.73	72583	160	0.85
MA3	3	0	320	192	0.80	72583	173	1.11
MA4[1]	3	0	320	42	0.83	72583	180	0.23
MB1	12	0	594	120	0.77	72583	167	0.72
MB2	1	0	1169	202	0.70	72583	153	1.32
MB3	3	0	791	170	0.79	72583	171	0.99
MB4	1	0	--	200	0.65	72583	142	1.41

1. Bearings that either failed prematurely or for which tensile properties are not available at zero lateral offset
2. Bearing with prior damage due to tension

Four of the sixteen bearings (DA1, DA3, MA1, and MA4) failed prematurely. Significant scatter is observed in the experimentally recorded value of the cavitation strength. Ideally, the cavitation strength should be obtained by applying a tensile load to a virgin bearing at zero lateral offset. However, the test protocols of the experimental program did not allow this procedure to be followed for all sixteen bearings. Some bearings were likely to have cavitation damage due to tests performed before the tensile tests, and in few other cases, the tensile test at zero lateral offset was not performed. In many cases, a well-defined post-cavitation response could not be obtained, which also introduces significant scatter in the calculated cavitation strength, but there is no more reliable a procedure. The theoretical value of cavitation strength ($=3GA$) is calculated using the shear modulus, G, and area for each bearing. The contribution of rubber cover is not included in calculation of area. If the outliers in the values of cavitation force are not considered, the experimental values show reasonable-to-good agreement with the theoretical predictions, noting that the shear modulus is calculated at somewhat arbitrary value of shear strain (e.g., 100%).

The experimentally determined tensile stiffness varies significantly for given geometry and rubber type. The secant tensile stiffness is sensitive to the length and the location of chord chosen on the tensile load-deformation curve for the calculation. The variation in tensile properties, including tensile stiffness and cavitation force is attributed to manufacturing. Better quality control would ensure that bearings of the same material and geometric construction would have similar mechanical properties, noting it's more difficult to maintain tight control for a small set of bearing of a non-standard size with thin steel shims and rubber layers.

The load-deformation behavior of an elastomeric bearing in tension is assumed to be elastic up to

cavitation with tensile stiffness equal to the compressive stiffness. The tensile properties calculated from the first cycle of loading and averaged for each bearing type are summarized in Table 8. A comparison of tensile and compression stiffness is also presented in Table 8. The averaged properties in Table 8 do not include bearings marked with the superscripts in Table 7.

There are differences between the tensile and compressive stiffness. However, the error in the calculated response of an isolation system is expected to be small from the use of equal stiffness in tension and compression, which allows the use of a linear model up to cavitation without much loss of accuracy.

Table 8: Average tensile properties of bearings

Bearing	F_c (kN)	u_c (mm)	β_v (%)	K_{v0} (kN/mm)		
				Tension	Compression	Difference (%)
DA	91	4	16.3	90	75	20
DB	98	2	6.7	257	393	35
MA	161	4	6.2	308	200	54
MB	173	2	5.9	851	772	9

The tensile stiffness decreases with increasing number of loading cycles. The reduction in stiffness depends on the change in tensile strain amplitude between consecutive cycles. If the tensile strain amplitude does not change significantly, the reduction in tensile stiffness is insignificant. Figure 13 shows the variation of tensile stiffness with number of cycles at different lateral offsets for bearing DA1, where Δ is the lateral offset and R is the radius of the bearing. The bearing is subjected to force controlled cyclic tests of an amplitude that was approximately half of the estimated cavitation strength. The tensile stiffness in Figure 13 does not change substantially because of small increments in the tensile strain amplitude between consecutive cycles. The tensile stiffness decreases substantially if the tensile strain amplitude between consecutive cycles increases significantly. Figure 14 shows the variation of tensile stiffness with number of cycles for bearing DB4, which was subjected to displacement controlled cyclic tensile tests with strain amplitude increasing every three cycles.

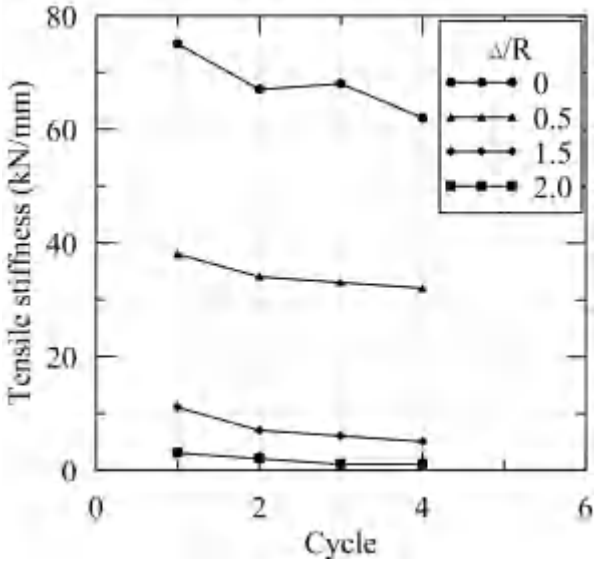

Figure 13: Variation of tensile stiffness with

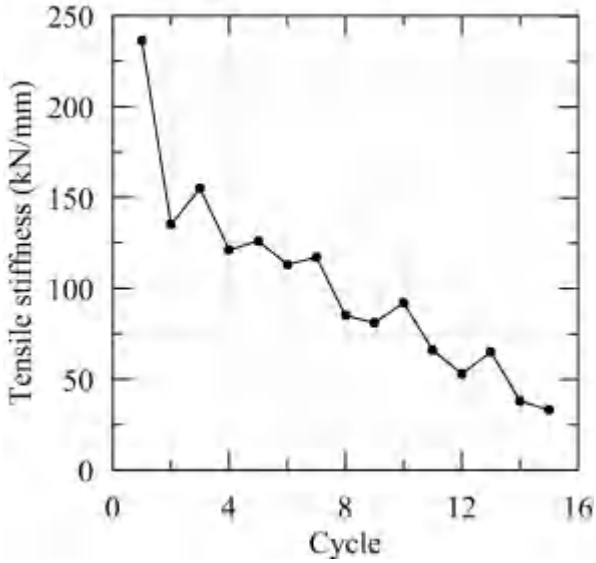

Figure 14: Variation of tensile stiffness with

number of cycles for bearing DA1 number of cycles for bearing DB4

4.2 Effect of Lateral Offset on Tensile Properties

The coupling of horizontal and vertical tensile responses was investigated by applying cyclic tensile loading to bearings at different offsets. The effect of lateral offset is assessed using three tensile properties: 1) pre- and post-cavitation tensile stiffness, 2) cavitation strength, and 3) hysteretic behavior in tension.

To determine the effect of lateral offset on pre-cavitation stiffness, four bearings (DA1, DA4, MA1, MA4) were subjected to force-controlled tensile loading cycles at different lateral offsets. The amplitude of the tensile loading was approximately half of the estimated cavitation strength. These bearings had not been damaged beforehand. The tensile load-deformation behavior of DA1 and DA4 at different values of lateral offsets is presented in Figure 15, where Δ is the lateral offset and R is the radius of the bearing. Bearings MA1 and MA4 failed prematurely due to debonding at the rubber-shim interface.

Although it is difficult to define and locate the exact point on the tensile force-deformation curve that corresponds to cavitation, the cavitation strength identified by a sharp reduction in tensile stiffness in Figure 15a and Figure 15b can be seen to be decreasing with lateral offset. This trend is consistent with the findings of Iwabe *et al.* [4] and Kato *et al.* [11]. The variation of tensile stiffness of bearings DA1 and DA4 with lateral offset is shown in Figure 16.

If force-controlled tests do not involve cavitation, increasing lateral offset increases hysteretic energy dissipation, as observed in Figure 15a and Figure 15b. An initial damage was induced in bearing DB1 by subjecting it to a tensile strain of 50%. Subsequently, two cyclic tensile tests were performed on DB1 with and without a lateral offset with tensile strain amplitude of 50%, so that any difference in hysteresis would only be because of lateral offset and not due to cavitation. Results are presented in Figure 17. No difference is observed.

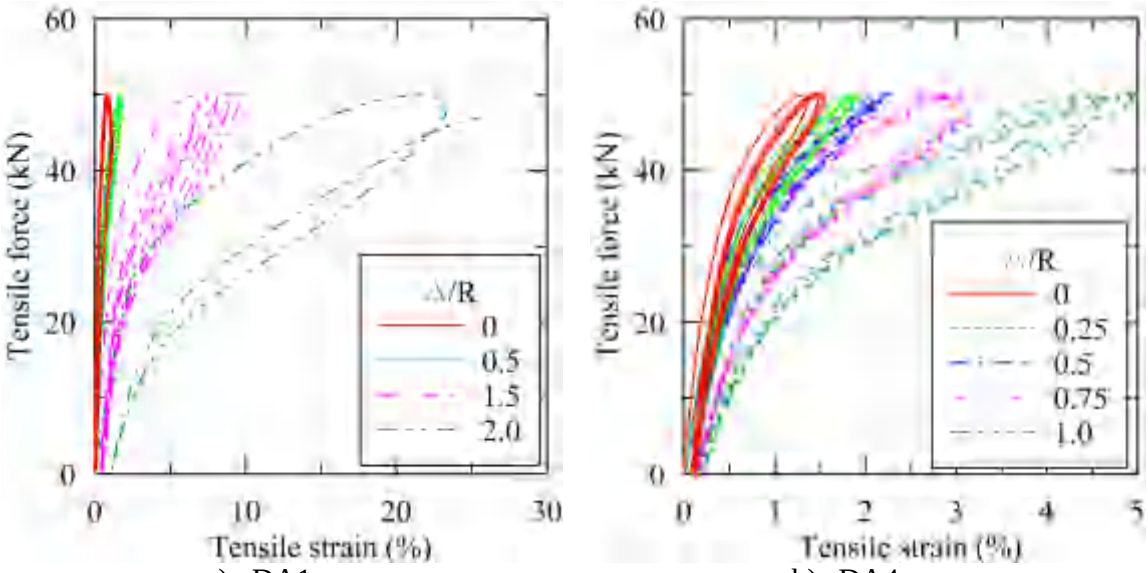

a) DA1 b) DA4

Figure 15: Load-deformation behavior in cyclic tensile loading at different lateral offsets

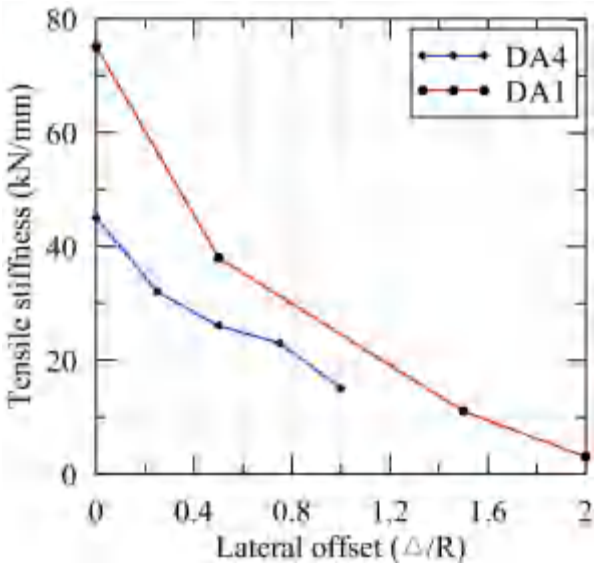

Figure 16: Variation of tensile stiffness with lateral offset strain

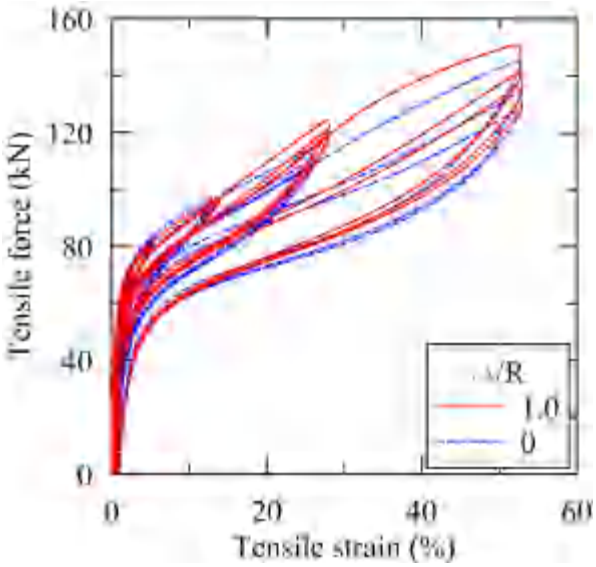

Figure 17: Effect of lateral offset on tensile hysteresis

4.3 Effect of Tensile Loading History on Cavitation

Past experiments have shown that damage in an elastomeric bearing accumulates with tensile deformation. Two test sequences, increasing triangular (IT) and decreasing triangular (DT), were used in which the tensile deformation amplitude was increased and decreased, respectively, after every three cycles. According to the mathematical model described in Kumar ***et al.*** [16], tensile properties such as the cavitation strength, the post-cavitation stiffness and the minimum value of cavitation strength, should only depend on the prior maximum value of tensile strain and not on the sequence of loading. The behavior of elastomeric bearings under cyclic tensile loading is presented in Figure 18.

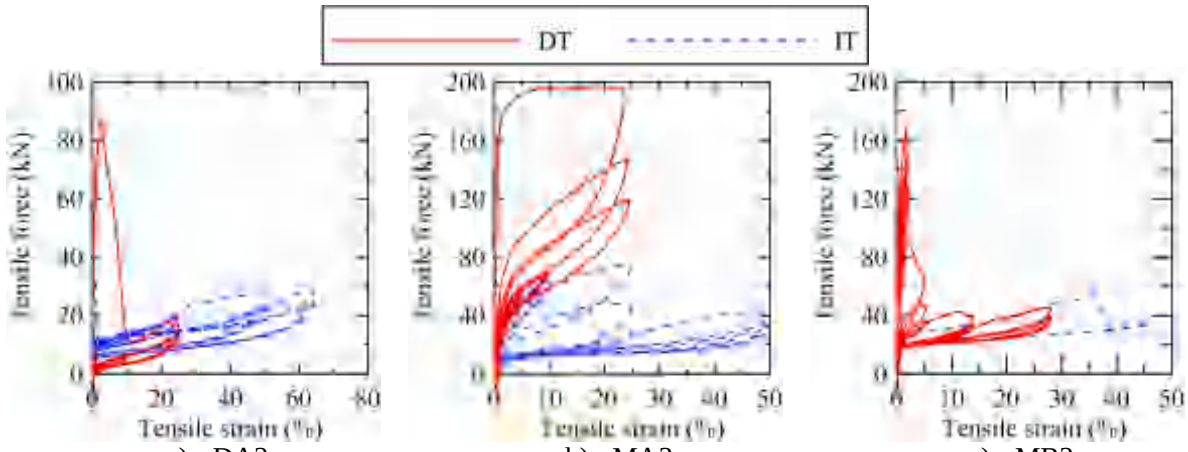

a) DA3 b) MA3 c) MB3

Figure 18: Behavior of elastomeric bearings under cyclic tensile loading

Differences are observed between the behaviors shown in Figure 18 and behavior observed from past experiments. Others (e.g. Iwabe ***et al.*** [4], Kato ***et al.*** [11], Warn [14]) have observed that if

the tensile strain exceeds the prior maximum value, the prior maximum value of the tensile force is recovered, and subsequently, tensile force increases with tensile strain. However, substantial reduction in force is observed between consecutive cycles for the bearings tested here, and the tensile force is not recovered after the tensile strain exceeds the prior maximum value. The reason for the different behavior is not known. A variety of factors, all related to manufacturing and the quality of product, could lead to the observed tensile behavior.

The residual strength observed in the tensile load-deformation curves of Figure 18 is due to the resistance of the 4 mm cover rubber around the perimeter of the circular bearings.

4.4 Effect of Cavitation on Mechanical Properties

The mechanical properties (shear modulus, axial stiffness, and damping ratios) of all sixteen bearings were monitored during the experiments. The effects of cavitation on mechanical properties were investigated through characterization tests before and after cavitation, including shear and compression tests. Results are presented in the following sections.

4.4.1 Shear Properties

The shear modulus and damping ratio of the bearings were monitored using shear characterization tests performed at 100% shear strain under an axial pressure of 1 MPa. Additional shear tests were conducted at other shear strain amplitudes and axial loads to investigate if the change in shear modulus following cavitation was sensitive to the shear strain and axial load. The changes in the shear properties of the bearings are summarized in Table 9.

Table 9: Pre- and post-cavitation shear properties of elastomeric bearings

Bearing	G_{eff} (MPa)			β_{eff} (MPa)	
	Pre-cavitation	Post-cavitation	Ratio	Pre-cavitation	Post-cavitation
DA1	0.40	0.37	0.93	4	5.1
DA2	0.42	0.40	0.95	4	4.4
DA3	0.42	0.40	0.96	5	3.8
DA4	0.38	0.36	0.94	4	4.9
DB1	n.a.[1]	0.44	n.a.	n.a.	3.5
DB2	n.a.	0.39	n.a.	n.a.	4.2
DB3	n.a.	0.41	n.a.	n.a.	5.6
DB4	0.45	0.43	0.96	3	3.8
MA1	0.80	n.a.	n.a.	5	n.a.
MA2	0.73	0.68	0.93	4	5.3
MA3	0.80	0.74	0.92	4	4.2
MA4	0.83	0.77	0.93	5	5.6
MB1	0.77	0.67	0.88	4	5.0
MB2	n.a.	0.70	n.a.	n.a.	7.8
MB3	0.79	0.71	0.90	4	5.6
MB4	n.a.	0.65	n.a.	n.a.	5.0

1. n.a.: not available

Others (e.g., Iwabe *et al.* [4]) have concluded that cavitation has no substantial effect on the shear modulus of a bearing because friction between the rubber layers provide adequate resistance to shear under nominal axial loads. The frictional resistance depends on the normal pressure and the contact area between the adjoining surfaces. The effect of cavitation on shear modulus may change with the magnitude of axial load maintained during shear tests and the shear strain at which effective shear modulus is calculated. To investigate this, cyclic shear tests were conducted before and after cavitation at various shear strain amplitudes and axial pressure. Results are presented in Figure 19.

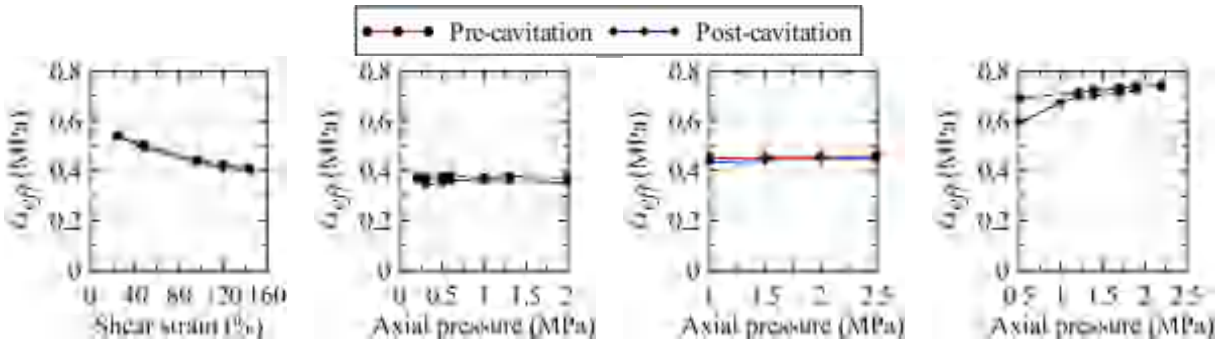

a) DB4 b) DA4 c) DB4 d) MB1

Figure 19: Variation of effective shear modulus with shear strain and axial pressure

The effect of cavitation on post-cavitation shear modulus of a bearing is consistent over the range of shear strain and axial pressure. At very low values of axial pressure (<0.5 MPa) differences between the pre- and post-cavitation shear modulus are seen because of the stick-slip motion across the failure surface after cavitation. Figure 20 is photograph of the bearing MA4 showing the slip across the ruptured interface under an axial pressure of 0.5 MPa. Slip is unlikely under a service axial pressure (≥3 MPa).

Figure 20: Slip across the failure surface in a post-cavitation shear test (bearing: MA4, axial pressure = 0.5 MPa)

4.4.2 Axial Properties

Force-controlled compression characterization tests were performed before and after cavitation to obtain compressive stiffness and damping ratio. The changes in axial properties in compression are summarized in Table 10. A very small reduction in compressive stiffness is

observed after cavitation. The pre- and post-cavitation values of the damping ratio in compression vary between 1 and 2% of critical.

Table 10: Pre- and post-cavitation axial properties of elastomeric bearings

Bearing	K_{v0} (MPa)			β_v (MPa)	
	Pre-cavitation	Post-cavitation	Ratio	Pre-cavitation	Post-cavitation
DA1	81	76	0.94	1.0	1.1
DA2	71	68	0.96	1.3	1.3
DA3	71	69	0.97	1.2	1.3
DA4	75	74	0.99	1.0	1.1
DB1	n.a.[1]	254	n.a.	n.a.	0.8
DB2	n.a.	285	n.a.	n.a.	0.9
DB3	n.a.	n.a.	n.a.	n.a.	n.a.
DB4	400	273	0.68	1.1	0.9
MA1	199	n.a.	n.a.	0.9	n.a.
MA2	216	161	0.74	1.5	1.1
MA3	209	191	0.91	1.5	1.5
MA4	196	180	0.92	1.6	1.4
MB1	686	605	0.88	2.2	1.0
MB2	n.a.	602	n.a.	n.a.	0.6
MB3	842	765	0.91	2.4	0.9
MB4	n.a.	519	n.a.	n.a.	1.2

1. n.a.: not available

4.4.3 Critical Buckling Load Capacity

A series of monotonic compression tests were performed at the end of tensile tests to investigate the effect of cavitation on the buckling load capacity of a bearing. The critical buckling load of all bearings were estimated from load-deformation curves in compression. The rated compressive load capacity of the testing machine is 1780 kN and its displacement capacity is 1.5 inches. Only eight of the sixteen bearings could be loaded to failure in compression. The buckling load for the remaining eight bearings exceeded 1780 kN. The ruptured halves of the bearings that failed during cavitation were re-assembled and a compressive load was applied.

Compressive load-deformation plots for the four types of bearing are presented in Figure 21. The initial plateau in the plots is due to a gap that the loading head of the testing machine had to overcome to engage the bearing. The axial displacement was measured using four linear potentiometers located symmetrically around bearings. The potentiometers read displacement values in the same direction up to buckling. However, once buckling begins, the signs sometimes reversed due to rotation of the bearing. Axial deformation is taken as the average reading of the four potentiometers. The apparent hardening is associated with lateral restraint to the bearing by the side walls of the testing machine following buckling.

The point on a load-deformation curve that corresponds to the beginning of buckling is shown with a solid black circle in Figure 21a and Figure 21c. For the DB and MB bearings, the critical

buckling loads were greater than the capacity of the testing machine (= 1780 kN) and they could not be failed in compression.

The theoretical values of critical buckling load obtained using the pre-cavitation and post-cavitation values of the effective shear modulus are presented in Table 11. No significant change in the buckling capacities of bearing types DA and MA due to cavitation is observed. Although failure could not be obtained for bearing type DB, they sustained a compressive load of 1700 kN, which is close to their theoretical buckling load, suggesting that there was no significant effect of cavitation on bearing type DB.

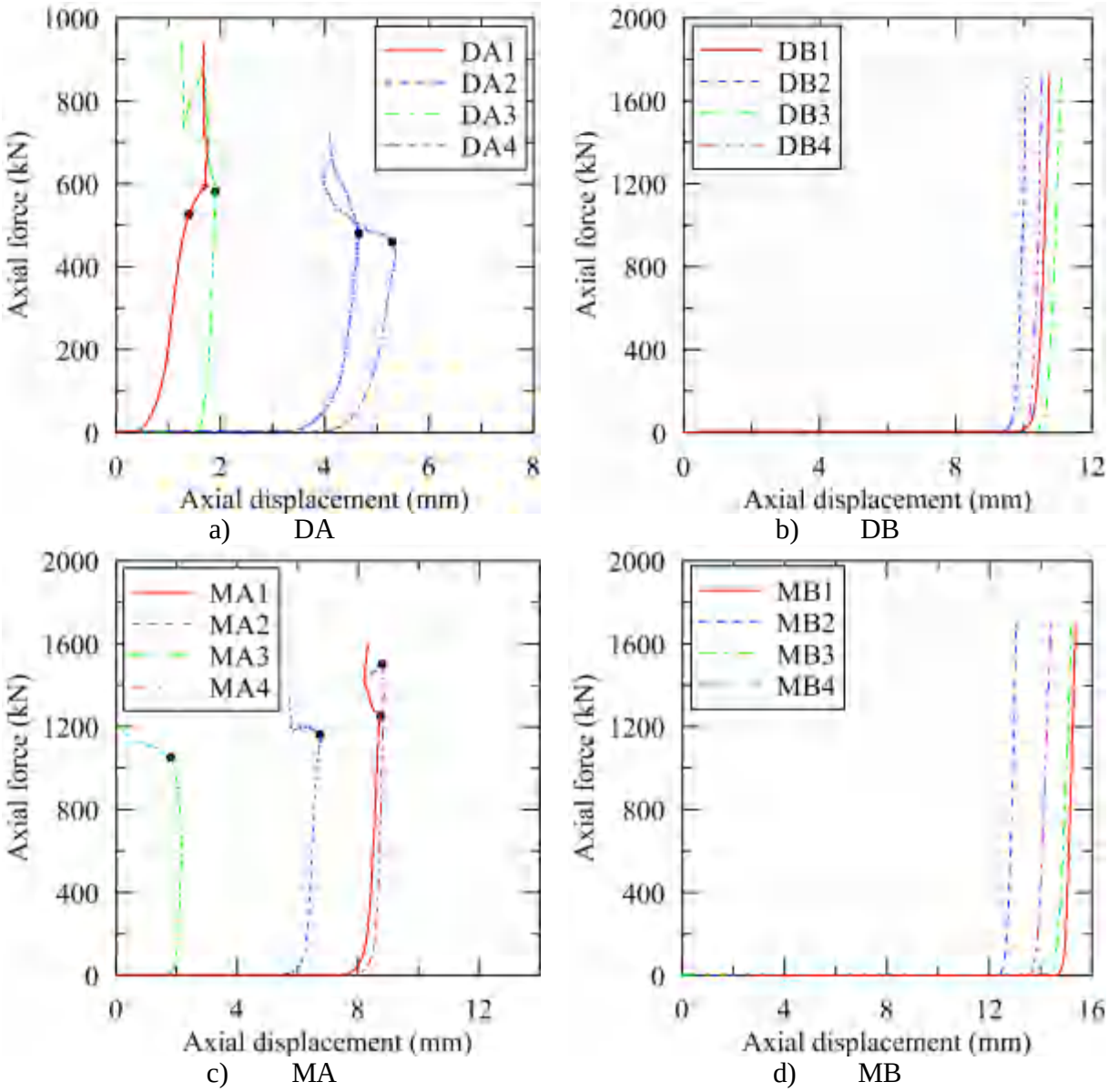

a) DA b) DB

c) MA d) MB

Figure 21: Compression failure tests of bearings

Table 11: Theoretical and experimental values of critical buckling load

Bearing	G_{eff} (MPa)		P_{cr} theoretical (kN)		P_{cr} experimental (kN)
	Before	After	Before	After	
DA1	0.40	0.37	544	505	525
DA2	0.42	0.40	570	544	580
DA3	0.42	0.40	570	544	480
DA4	0.38	0.36	518	492	460
DB1	n.a.	0.44	n.a.	1643	>1780
DB2	n.a.	0.39	n.a.	1480	>1780
DB3	n.a.	0.41	n.a.	1546	>1780
DB4	0.45	0.43	1675	1611	>1780
MA1	0.80	n.a.	1280	n.a.	1250
MA2	0.73	0.68	1182	1111	1160
MA3	0.80	0.74	1280	1196	1050
MA4	0.83	0.77	1321	1238	1500
MB1	0.77	0.67	3060	2757	>1780
MB2	n.a.	0.70	n.a.	2850	>1780
MB3	0.79	0.71	3118	2880	>1780
MB4	n.a.	0.65	n.a.	2694	>1780

4.4.4 Failure Mode in Tension

The failure mode of a bearing is defined here as the loading conditions under which the bearing fails (e.g., pure tension, tension with lateral offset). The failure mechanism describes how the failure begins. The description of failure for each bearing in tension is presented in Figure 21, where ε_t is the tensile strain and Δ is the co-existing lateral offset.

The most common failure type in the DIS bearings was the formation of cavities in the rubber layer, whereas the Mageba bearings failed due to debonding at the interface of a rubber layer and a steel shim. Failure through formation of cavities in the volume of the rubber is the preferred mechanism. These two failure mechanisms are shown in Figure 23.

Four of the sixteen bearings, DA1 (0.53), DA4 (0.55), MA1 (0.09), and MA4 (0.23), failed prematurely (failure occurred below theoretical cavitation force), where the value in parentheses is the ratio of the experimental to theoretical cavitation strengths. Although most of the experimental work to date (e.g., Iwabe *et al.* [4], Kato *et al.* [11], Warn [14]) on cyclic loading of elastomeric bearings report a tensile deformation capacity of more than 100%, few bearings here achieved this. The hysteretic behavior was also different than what has been observed in past experimental studies.

a) DA1_13
ε_t = 25%, Δ / R = 2

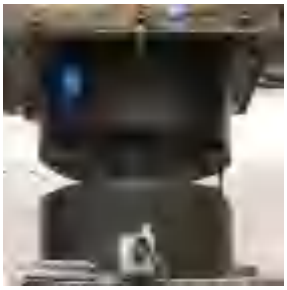

b) DA2_3a
ε_t = 50%, Δ / R = 0

c) DA3_06
ε_t = 65%, Δ / R = 0

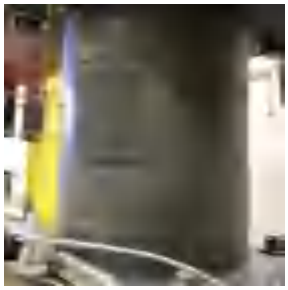

d) DA4_14
ε_t = 25%, Δ / R = 0

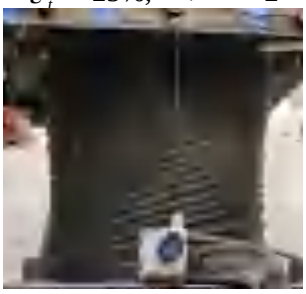

e) DB1_14
ε_t = 93%, Δ / R = 0

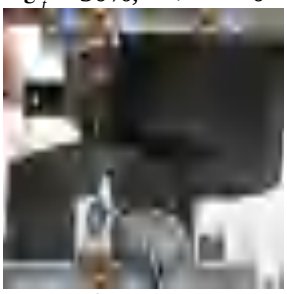

f) DB2_01
ε_t = 15%, Δ / R = 1

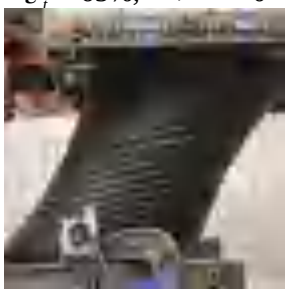

g) DB4_21
ε_t = 100%, Δ / R = 1

h) MA1_08
ε_t = 25%, Δ / R =0

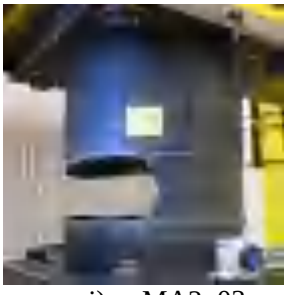

i) MA2_03
ε_t = 65%, Δ / R = 0

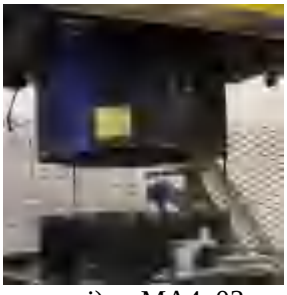

j) MA4_03
ε_t = 50%, Δ / R = 0

k) MB2_01
ε_t = 100%, Δ / R = 0

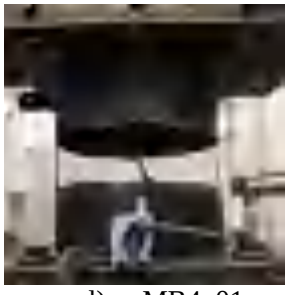

l) MB4_01
ε_t = 50%, Δ / R = 0

Figure 22: Failure state of bearings under tension

a) Cavities in the rubber volume (DA2)

b) Debonding at rubber-shim interface (MA4)

Figure 23: Failure mechanism in rubber bearings under tension

5. Experimental validation

Kumar *et al.* [16] describe the mechanism of damage initiation and propagation over time and proposed a mathematical model that predicts the behavior of an elastomeric bearing under cyclic tensile loading. The following assumptions are investigated:

1. Cavitation strength decreases (damage increases) with increasing values of tensile strain amplitude of each cycle.
2. No additional damage is observed if tensile strain is less than its prior maximum value.
3. If the prior maximum value of tensile strain is exceeded, the formation of new cavities leads to additional damage, and cavitation strength is further decreased.
4. Cavitation strength converges to a minimum value.

A comparison of the experimental behavior and numerical results obtained using the phenomenological model described in Kumar *et al.* [16] is presented in Figure 24 for all sixteen bearings, where F/F_c is the tensile force normalized by the cavitation strength. The values of the parameters used for the tensile model are: cavitation parameter, k = 20, 2) strength degradation parameter, a = 1.0, and 3) damage index, ϕ_{max} = 0.9.

Numerical results show reasonable agreement with experimental behavior in most cases. Differences are observed in a few cases between the behaviors shown in Figure 24 and those observed from past experiments (e.g. [4], [14], [11]). It has been observed in previous experimental studies that if the tensile strain exceeds the prior maximum value, the prior maximum value of the tensile force is recovered, and subsequently, tensile force increases with tensile strain. However, force reduction is observed between consecutive cycles for a few bearings tested here, and the tensile force is not recovered after tensile strain exceeds the prior maximum value. The force reduction might be due to initiation of tensile failure. It is difficult to locate the precise point of failure on the load-deformation curve up to which the phenomenological model can applied. A consistent failure strain in tension is not observed among all the bearings. The tensile strain capacities of the bearings are smaller than those reported by others (e.g., [4], [14], [11], [10]).

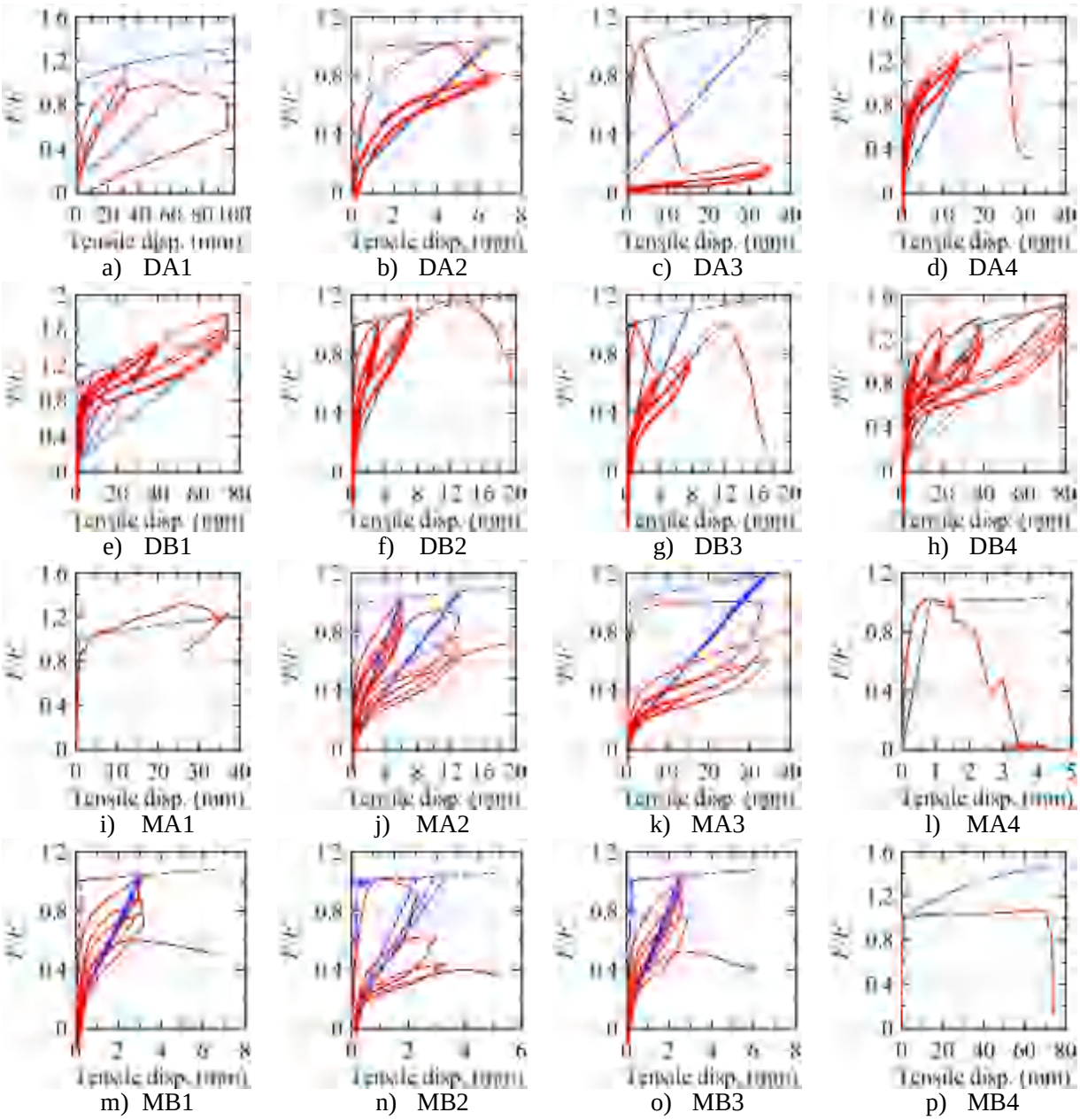

Figure 24: Validation of the mathematical model in tension, normalized force versus displacement

6. Summary and conclusions

The key conclusions of the experiments are:

1. The value of $3GA$ is a reasonable estimate of the cavitation strength of a bearing.
2. The pre-cavitation tensile stiffness of a bearing decreases with an increasing number of loading cycles. The magnitude of the reduction depends on the prior maximum value of the tensile strain.
3. The pre-cavitation tensile stiffness decreases with an increase in coexisting shear strain.

4. Cavitation strength decreases with co-existing shear strain.
5. The sequence of loading does not change the behavior of elastomeric bearing under cyclic tension.
6. There is an insignificant change from a practical perspective in the compressive stiffness of a bearing following cavitation.
7. Cavitation has no significant effect on the effective shear modulus of a bearing for shear strain less than 150% under axial compressive pressure greater than 1 MPa.
8. No significant reduction in the buckling load of a bearing is observed due to prior cavitation.

Good quality assurance (QA) and quality control (QC) is key to the use of elastomeric bearings to seismically isolate nuclear power plants. Mathematical models are formulated based on physics and behaviors observed in experiments. These mathematical models are developed using a set of generalized assumptions about the expected behavior of elastomeric bearings. The desirable behavior of an elastomeric bearing in tension includes:

1. Cavitation at a well-defined force that is reproducible across similar bearings
2. Sufficient tensile deformation capacity
3. Ability to recover strength if tensile deformation exceeds the prior maximum value
4. Final failure through formation of cavities in the volume of the rubber and not through de-bonding at the interface of a rubber layer and a steel shim.

The bearings tested for the study described in this paper showed different characteristics from those tested previously, including a) smaller tensile strain capacity, b) reduction in peak tensile force in consecutive cycles to a specified tensile displacement, and c) reduction in tensile resistance for loading to tensile strain that exceed a prior maximum value. These differences are attributed to QA and QC, noting that bearing manufacturers very rarely fabricate isolators of the relatively small size tested here. The infrequent manufacture of small runs of bearings with geometries most different from commercial product make it extremely difficult to achieve the high quality expected of isolators for nuclear power plant applications.

ACKNOWLEDGEMENT

This research project is supported by a grant to MCEER from the United States Nuclear Regulatory Commission (USNRC) and the Lawrence Berkeley National Laboratory (LBNL). This financial support is gratefully acknowledged. The authors thank Dr. Annie Kammerer, formerly of the USNRC, and Dr. Robert Budnitz of LBNL for their technical contributions to the research project, and to Dynamic Isolation Systems, Inc. and Mageba for contributing bearings for the tests.

REFERENCES

[1] Japan Road Association (JRA). (2012). "Bearing support design guide for highway bridges (In Japanese)." Japan.

[2] Comité Européen de Normalisation (CEN). (2005). "Eurocode 8: Design of structures for earthquake resistance-Part 2: Bridges." *EN 1998-2*, Brussels, Belgium.

[3] Ministry of Construction of the People's Republic of China, China Architecture & Building Press (MOCPRC). (2010). "Code for seismic design of buildings (in Chinese)." *GB50011-2010*, Beijing, China

[4] Iwabe, N., Takayama, M., Kani, N., and Wada, A. (2000). "Experimental study on the effect of tension for rubber bearings." *Proceedings: 12th World Conference on Earthquake Engineering*, New Zealand.

[5] American Society of Civil Engineers (ASCE). (forthcoming). "Seismic analysis of safety-related nuclear structures and commentary." *ASCE 4-14*, Reston, VA.

[6] United States Nuclear Regulatory Commission (USNRC). (forthcoming). "Technical considerations for seismic isolation of nuclear facilities." *NUREG-xxxx*, Washington DC.

[7] Gent, A. N., and Lindley, P. B. (1959). "Internal rupture of bonded rubber cylinders in tension." *Proceedings of the Royal Society of London, Series A, Mathematical and Physical Sciences*, 249(1257), 195-205.

[8] Dorfmann, A., and Burtscher, S. L. (2000). "Aspects of cavitation damage in seismic bearings." *Journal of Structural Engineering*, 126(5), 573-579.

[9] Dorfmann, A. (2003). "Stress softening of elastomers in hydrostatic tension." *Acta Mechanica*, 165(3-4), 117-137.

[10] Clark, P. W. (1996). "Experimental studies of the ultimate behavior of seismically-isolated structures." Ph.D. Dissertation, University of California at Berkeley, CA.

[11] Kato, R., Oka, K., and Takayama, M. (2003). "The tensile tests of natural rubber bearings focused on the effect of the steel flange plates." *Proceedings: Pressure Vessels and Piping Conference*, American Society of Mechanical Engineers, Cleveland, OH, 81-88.

[12] Shoji, G., Saito, K., Kameda, T., and Fueki, T. (2004). "Seismic performance of a laminated rubber bearing under tensile axial loading." *Proceedings: 13th World Conference on Earthquake Engineering*, August 1-6, 2004, Vancouver, Canada.

[13] Feng, D., Miyama, T., Lu, X., and Ikenaga, M. (2004). "A shaking table test study on shear tensile properties of lead rubber bearings." *Proceedings: 13th World Conference on Earthquake Engineering*, August 1-6, 2004, Vancouver, Canada.

[14] Warn, G. P. (2006). "The coupled horizontal-vertical response of elastomeric and lead-rubber seismic isolation bearings." Ph.D. Dissertation, The State University of New York at Buffalo, Buffalo, NY.

[15] Constantinou, M. C., Whittaker, A. S., Kalpakidis, Y., Fenz, D. M., and Warn, G. P. (2007). "Performance of seismic isolation hardware under service and seismic loading." MCEER-07-0012, Multidisciplinary Center for Earthquake Engineering Research, State University of New York at Buffalo, NY.

[16] Kumar, M., Whittaker, A., and Constantinou, M. (2014). "An advanced numerical model of elastomeric seismic isolation bearings." *Earthquake Engineering & Structural Dynamics*, 43(13), 1955-1974.

[17] McKenna, F., Fenves, G., and Scott, M. (2006). "OpenSees: Open system for earthquake engineering simulation." Pacific Earthquake Engineering Center, University of California, Berkeley, CA., (http://opensees.berkeley.edu).

[18] Dassault (2010). Computer Program ABAQUS/CAE, Dassault Systèmes, Providence, RI.

[19] LSTC (2012). Computer Program LS-DYNA, Livermore Software Technology Corporation, Livermore, CA.

[20] Kumar, M. (2015). "Seismic isolation of nuclear power plants using elastomeric bearings." Ph.D. Dissertation, University at Buffalo, The State University of New York, Buffalo, NY.

[21] American Association of State Highway and Transportation Officials (AASHTO). (1999). "Guide Specification for Seismic Isolation of Bridges." Washington, D.C.

[22] Comité Européen de Normalisation (CEN). (2009). "Anti-seismic devices." *EN 15129*, Brussels, Belgium.

[23] Lindley, P. B. (1992). "Engineering design with natural rubber." Malaysian Rubber Producers Association.

[24] Fuller, K. N. G., Gregory, M. J., Harris, J. A., Muhr, A. H., and Roberts, A. D. (1988). "Engineering use of natural rubber." Oxford University Press, New York, NY.

[25] Stanton, J. F., Roeder, C. W., Mackenzie-Helnwein, P., White, C., Kuester, C., and Craig, B. (2008). "Rotaton limits for elastomeric bearings." NCHRP-596, National Cooperative Highway Research Program, Seattle, WA.

[26] Kelly, J. M., and Lai, J. W. (2011). "The use of tests on high-shape-factor bearings to estimate the bulk modulus of natural rubber." *Seismic Isolation and Protective Systems*, 2(1), 21-33.

[27] SEESL (2014). <http://nees.buffalo.edu/training/krypton/geoloc%20English.PDF>. (19 June, 2014).

[28] Warn, G. P., Whittaker, A. S., and Constantinou, M. C. (2007). "Vertical stiffness of elastomeric and lead-rubber seismic isolation bearings." *Journal of Structural Engineering*, 133(9), 1227-1236.

[29] Warn, G. P., and Whittaker, A. S. (2006). "A study of the coupled horizontal-vertical behavior of elastomeric and lead-rubber seismic isolation bearings." MCEER-06-0011, Multidisciplinary Center for Earthquake Engineering Research, State University of New York at Buffalo, NY.

[30] Kelly, J. M. (1993). "Earthquake-resistant design with rubber." Springer-Verlag, London.